Wave-aberration control with a liquid crystal on silicon (LCOS) spatial phase modulator

Enrique J. Fernández, Pedro M. Prieto and Pablo Artal

*Laboratorio de Optica, Centro de Investigación en Optica y Nanofísica, Universidad de Murcia,
Campus de Espinardo, 30071 Murcia, Spain*
enriquej@um.es, pegrito@um.es, pablo@um.es

Abstract: Liquid crystal on Silicon (LCOS) spatial phase modulators offer enhanced possibilities for adaptive optics applications in terms of response velocity and fidelity. Unlike deformable mirrors, they present a capability for reproducing discontinuous phase profiles. This ability also allows an increase in the effective stroke of the device by means of phase wrapping. The latter is only limited by the diffraction related effects that become noticeable as the number of phase cycles increase. In this work we estimated the ranges of generation of the Zernike polynomials as a means for characterizing the performance of the device. Sets of images systematically degraded with the different Zernike polynomials generated using a LCOS phase modulator have been recorded and compared with their theoretical digital counterparts. For each Zernike mode, we have found that image degradation reaches a limit for a certain coefficient value; further increase in the aberration amount has no additional effect in image quality. This behavior is attributed to the intensification of the 0-order diffraction. These results have allowed determining the usable limits of the phase modulator virtually free from diffraction artifacts. The results are particularly important for visual simulation and ophthalmic testing applications, although they are equally interesting for any adaptive optics application with liquid crystal based devices.

©2009 Optical Society of America

OCIS codes: (010.1080) Adaptive optics; (330.4460) Ophthalmic optics; (330.5370) Physiological optics.

References and links

1. R. Dou and M. K. Giles, "Closed-loop adaptive optics system with a liquid crystal television as a phase retarder," Opt. Lett. **20**, 1583–1585 (1995).
2. G. D. Love, "Wave-front correction and production of Zernike modes with a liquid-crystal spatial light modulator," Appl. Opt. **36**, 1517–1524 (1997).
3. J. Gourlay, G. D. Love, P.M. Birch, R.M. Sharples, and A. Purvis, "A real time closed loop liquid crystal adaptive optics system: first results," Opt. Commun. **137**, 17-21 (1997).
4. D. C. Dayton, S. P. Sandven, J.D. Gonglewski, S. Browne, S. Rogers, and S. Mcdermott, "Adaptive optics using a liquid crystal phase modulator in conjunction with a Shack-Hartmann wave-front sensor and zonal control algorithm," Opt Express **1**, 338-346 (1997),
http://www.opticsexpress.org/abstract.cfm?URI=OPEX-1-11-338.
5. F. H. Li, N. Mukohzaka, N. Yoshida, Y. Igasaki, H. Toyoda, T. Inoue, Y. Kobayashi, and T Hara, "Phase modulation characteristics analysis of optically-addressed parallel-aligned nematic liquid crystal phase-only spatial light modulator combined with a liquid crystal display," Opt. Rev. **5**, 174-178 (1998).
6. A. Neil, M. J. Booth, and T. Wilson, "Dynamic wave-front generation for the characterization and testing of optical systems," Opt. Lett. **23**, 1849-1851 (1998).
7. S. R. Restaino, D. C. Dayton, S. L. Browne, J. Gonglewski, J. Baker, S. Rogers, S. Mcdermott, J. Gallegos, and M. Shilko, "One the use of dual frequency nematic material for adaptive optics systems: first results of a closed-loop experiment," Opt. Express **6**, 2-7 (2000),
http://www.opticsexpress.org/abstract.cfm?URI=OPEX-6-1-2.
8. D. C. Dayton, S. L. Browne, J. D. Gonglewski, and S. R. Restaino, "Characterization and control of a multielement dual-frequency liquid-crystal device for high-speed adaptive optical wave-front correction," Appl. Opt. **40**, 2345-2355 (2001).

9. S. Kotova, M. Kvashnin, M. Rakhmatulin, O. Zayakin, I. Guralnik, N. Klimov, P. Clark, G. Love, A. Naumov, C. Saunter, M. Loktev, G. Vdovin, and L. Toporkova, "Modal liquid crystal wavefront corrector," Opt. Express **10**, 1258-1272 (2002), http://www.opticsinfobase.org/abstract.cfm?URI=oe-10-22-1258.

10. P. M. Prieto, E. J. Fernández, S. Manzanera, and P. Artal, "Adaptive Optics with a programmable phase modulator: applications in the human eye," Opt. Express **12**, 4059-4071 (2004), http://www.opticsinfobase.org/oe/abstract.cfm?URI=oe-12-17-4059.

11. L. Hu, L. Xuan, Y. Liu, Z. Cao, D. Li, and Q. Mu, "Phase-only liquid crystal spatial light modulator for wavefront correction with high precision," Opt. Express **12**, 6403-6409 (2004), http://www.opticsinfobase.org/abstract.cfm?URI=oe-12-26-6403.

12. Y. Liu, Z. Cao, D. Li, Q. Mu, L. Hu, X. Lu, and L. Xuan, "Correction for large aberration with phase-only liquid-crystal wavefront corrector," Opt. Eng. **45**, 128001-128005 (2006).

13. J. Arines, V. Durán, Z. Jaroszewicz, J. Ares, E. Tajahuerce, P. Prado, J. Lancis, S. Bará, and Vicent Climent, "Measurement and compensation of optical aberrations using a single spatial light modulator," Opt. Express **15**, 15287-15292 (2007), http://www.opticsinfobase.org/abstract.cfm?URI=oe-15-23-15287.

14. G. Vdovin and P. M. Sarro, "Flexible mirror micromachined en silicon," Appl. Opt. **29**, 2968-2972 (1995).

15. L. Zhu, P-C. Sun, and Y. Fainman, "Aberration-free dynamic focusing with a multichannel micromachined membrane deformable mirror," Appl. Opt. **38**, 5350-5354 (1999).

16. D. Dayton, S. Restaino, J. Gonglewski, J. Gallegos, S. McDermott, S. Browne, S. Rogers, M. Vaidyanathan, and M. Shilko, "Laboratory and field demonstration of low cost membrane mirror adaptive optics system," Opt. Commun. **176**, 339-345 (2000).

17. C. Paterson, I Munro, and J. C. Dainty, "A low cost adaptive optics system using a membrane mirror," Opt. Express **6**, 175-185 (2000), http://www.opticsinfobase.org/oe/abstract.cfm?URI=oe-6-9-175.

18. N. Doble, G. Yoon, L. Chen, P. Bierden, B. Singer, S. Olivier, and D. R. Williams, "Use of a microelectromechanical mirror for adaptive optics in the human eye," Opt. Lett. **27**, 1537-1539 (2002).

19. E. J. Fernández and P. Artal, "Membrane deformable mirror for adaptive optics: performance limits in visual optics," Opt. Express **11**, 1056-1069 (2003), http://www.opticsinfobase.org/oe/abstract.cfm?URI=oe-11-9-1056.

20. E. Dalimier and C. Dainty, "Comparative analysis of deformable mirrors for ocular adaptive optics," Opt. Express **13**, 4275-4285 (2005), http://www.opticsinfobase.org/abstract.cfm?URI=oe-13-11-4275.

21. E. J. Fernández, L. Vabre, B. Hermann, A. Unterhuber, B. Povazay, and W. Drexler, "Adaptive optics with a magnetic deformable mirror: applications in the human eye," Opt. Express **14**, 8900-8917 (2006), http://www.opticsinfobase.org/oe/abstract.cfm?URI=oe-14-20-8900.

22. P. A. Piers, S. Manzanera, P. M. Prieto, N. Gorceix, and Pablo Artal, "Use of adaptive optics to determine the optimal ocular spherical aberration," J. Cataract Refract. Surg. **33**, 1721-1726 (2007).

23. L. Lundström, S. Manzanera, P. M. Prieto, D. B. Ayala, N. Gorceix, J. Gustafsson, P. Unsbo, and P. Artal, "Effect of optical correction and remaining aberrations on peripheral resolution acuity in the human eye," Opt. Express **15**, 12654-12661 (2007), http://www.opticsinfobase.org/oe/abstract.cfm?URI=oe-15-20-12654.

24. D. C. Dayton, S. L. Browne, S. P. Sandven, J. D. Gonglewski, and A. V. Kudryashov,, "Theory and laboratory demonstrations on the use of a nematic liquid-crystal phase modulator for controlled turbulence generation and adaptive optics," Appl. Opt. **37**, 5579-5589 (1998).

25. D. Dayton, J. Gonglewski, S. Restaino, J. Martin, J. Phillips, M. Hartman, P. Kervin, J. Snodgress, S. Browne, N. Heimann, M. Shilko, R. Pohle, B. Carrion, C. Smith, and D. Thiel, "Demonstration of new technology MEMS and liquid crystal adaptive optics on bright astronomical objects and satellites," Opt. Express **10**, 1508-1519 (2002), http://www.opticsinfobase.org/abstract.cfm?URI=oe-10-25-1508.

26. E. J. Fernández, B. Povazay, B. Hermann, A. Unterhuber, H. Sattmann, P. M. Prieto, R. Leitgeb, P. Ahnelt, P. Artal, and W. Drexler, "Three-dimensional adaptive optics ultrahigh-resolution optical coherence tomography using a liquid crystal spatial light modulator," Vision Res. **45**, 3432–3444 (2005).

27. F. Vargas-Martín, P. M. Prieto, and P.Artal, "Correction of the aberrations in the human eye with a liquid crystal spatial light modulator: limits to performance," J. Opt. Soc. Am. A **15**, 2552-2562 (1998).

28. E. J. Fernández, S. Manzanera, P. Piers, and P. Artal, "Adaptive optics visual simulator," J. Refrac. Surg. **18**, 634-638 (2002).

29. P. Artal, L. Chen, E. J. Fernández, B. Singer, S. Manzanera, and D. R. Williams, "Neural compensation for the eye's optical aberrations," J. Vision **4**, 281-287 (2004), http://journalofvision.org/4/4/4/, doi:10.1167/4.4.4.

30. E. J. Fernández and P. Artal, "Study on the effects of monochromatic aberrations in the accommodation response by using adaptive optics," J. Opt. Soc. of Am. A **22**, 1732-1738 (2005).

31. P. Piers, E. J. Fernández, S. Manzanera, S. Norrby, and P. Artal, "Adaptive optics simulation of intraocular lenses with modified spherical aberration," Invest. Ophthalmol. Visual Sci. **45**, 4601-4610 (2004).

32. S. Manzanera, P. M. Prieto, D. B. Ayala, J. M. Lindacher, and P. Artal, "Liquid crystal Adaptive Optics Visual Simulator: Application to testing and design of ophthalmic optical elements," Opt. Express **15**, 16177-16188 (2007), http://www.opticsinfobase.org/oe/abstract.cfm?URI=oe-15-24-16177.

33. V. Durán, V. Climent, E. Tajahuerce, Z. Jaroszewicz, J. Arines, and S. Bará, "Efficient compensation of Zernike modes and eye aberration patterns using low-cost spatial light modulators," J. Biomed. Opt. **12**, 14037-14043 (2007).

34. Q. Mu, Z. Cao, D. Li, L. Hu, and L. Xuan, "Liquid Crystal based adaptive optics system to compensate both low and high order aberrations in a model eye," Opt. Express **15**, 1946-1953 (2007), http://www.opticsinfobase.org/abstract.cfm?URI=oe-15-4-1946.

35. D. Miller, L. Thibos, and X. Hong, "Requirements for segmented correctors for diffraction-limited performance in the human eye," Opt. Express **13**, 275-289 (2005), http://www.opticsinfobase.org/abstract.cfm?URI=oe-13-1-275.

36. W. Hossack, E. Theofanidou, J. Crain, K. Heggarty, and M. Birch, "High-speed holographic optical tweezers using a ferroelectric liquid crystal microdisplay," Opt. Express **11**, 2053-2059 (2003), http://www.opticsinfobase.org/oe/abstract.cfm?URI=oe-11-17-2053.

37. A. Lafong, W. J. Hossack, J. Arlt, T. J. Nowakowski, and N. D. Read, "Time-Multiplexed Laguerre-Gaussian holographic optical tweezers for biological applications," Opt. Express **14**, 3065-3072 (2006), http://www.opticsinfobase.org/oe/abstract.cfm?URI=oe-14-7-3065.

38. X. Wang, B. Wang, J. Pouch, F. Miranda, J. E. Anderson, P. J. Bos, "Performance evaluation of a liquid-crystal-on-silicon spatial light modulator," Opt. Eng. **43**, 2769-2774 (2004).

39. Q. Mu, Z. Cao, L. Hu, D. Li, and L. Xuan, "An adaptive optics imaging system based on a high-resolution liquid crystal on silicon device," Opt. Express **14**, 8013-8018 (2006), http://www.opticsinfobase.org/abstract.cfm?URI=oe-14-18-8013.

40. Z. Cao, Q. Mu, L. Hu, D. Li, Y. Liu, L. Jin, and L. Xuan, "Correction of horizontal turbulence with nematic liquid crystal wavefront corrector," Opt. Express **16**, 7006-7013 (2008), http://www.opticsinfobase.org/abstract.cfm?URI=oe-16-10-7006.

41. Q. Mu, Z. Cao, D. Li, L. Hu, and L. Xuan, "Open-loop correction of horizontal turbulence: system design and result," Appl. Opt. **47**, 4297-4301 (2008).

42. H. Hofer, P. Artal, B. Singer, J. L. Aragón, and D. R. Williams, "Dynamics of the eye's wave aberration," J. Opt. Soc. Am. A **18**, 497-506 (2001).

43. K. M. Hampson, I. Munro, C. Paterson, and C. Dainty, "Weak correlation between the aberration dynamics of the human eye and the cardiopulmonary system," J. Opt. Soc. Am. A **22**, 1241-1250 (2005).

44. R. J. Noll, "Zernike polynomials and atmospheric turbulence," J. Opt. Soc. Am. **66**, 207-211 (1976).

45. J. Liang, B. Grimm, S. Goelz, and J. F. Bille, "Objective measurement of wave aberrations of the human eye with the use of a Hartmann–Shack wave-front sensor," J. Opt. Soc. Am. A **11**, 1949–1957 (1994).

46. J. Liang and D. R. Williams, "Aberrations and retinal image quality of the normal human eye," J. Opt. Soc. Am. A **14**, 2873–2883 (1997).

47. P. M. Prieto, F. Vargas-Martín, S. Goelz, P. Artal, "Analysis of the performance of the Hartmann-Shack sensor in the human eye," J. Opt. Soc. Am. A **17**, 1388-1398 (2000).

48. J.W. Goodman, *Introduction to Fourier optics*, 3rd Edition, (Roberts and Company, Publishers, Englewood, CO, 2005).

49. P. Artal, "Calculations of the 2-dimensional foveal retinal images in real eyes," J. Opt. Soc. Am. A **7**, 1374-1381 (1990).

50. R. Román, J. J. Quesada, and J. Martínez, "Multiresolution-information analysis for images," Signal Process. **24**, 77-91 (1991).

51. E. N. Kirsanova and M. G. Sadovsky, ""Entropy approach in the analysis of anisotropy of digital images," Open Syst. Inf. Dyn. **9**, 239-250 (2002).

52. P. Marziliano, F. Dufaux, S. Winkler, and T. Ebrahimi, "Perceptual blur and ringing metrics: application to JPEG2000," Signal Process. **19**, 163-172 (2004).

53. S. Gabarda and G. Cristóbal, "Blind image quality assessment through anisotropy," J. Opt. Soc. Am. A **24**, 42-51 (2007).

54. J. S. McLellan, P. M. Prieto, S. Marcos, S. A. Burns, "Effects of interactions among wave aberrations on optical image quality," Vision Res. **46**, 3009-3016 (2006).

55. P. M. Prieto, F. Vargas-Martín, J. S. McLellan, and S. A. Burns, "Effect of the polarization on ocular wave aberration measurements," J. Opt. Soc. Am. A **19**, 809–814 (2002).

1. Introduction

In recent years, different types of phase modulators based on the use of liquid crystal have been developed and tested as aberration correctors [1-13]. The principle of operation of these devices is relatively simple. Phase is modulated by spatially changing the refractive index of the liquid crystal, consequently modifying the optical path of the incident light. This effect is

achieved by applying an electrical field to the material. The molecules, initially aligned parallel to each other, respond to the field with a rotation which causes an effective change in the macroscopic refractive index. Liquid crystal phase modulators provide an interesting alternative to conventional deformable mirrors [14-23]. The number of independent elements to control the phase in liquid crystal-based modulators currently is 3-4 orders of magnitude superior to deformable mirrors, the latter typically in the order of 100. In addition, phase modulators do not present the continuity constrains that limit the capability of deformation of flexible membranes in mirrors. This feature can be exploited to significantly increase the effective stroke by using 2π-wrapped phase maps, and also extends the range of achievable phase manipulations to discontinuous surfaces. Among the disadvantages of liquid crystal phase modulators, the response speed (traditionally 4-5 Hz) is typically pointed out. This has been overcome in part with the recently developed liquid crystal on silicon (LCOS) technology, which allows up to 60 Hz. Another cited drawback is the requirement of linearly polarized light, although that is irrelevant from the point of view of aberration control.

In the context of adaptive optics, liquid crystal phase modulators have been used in Astronomy, correcting the atmospheric turbulence [24,25], in order to enhance the optical quality of the astronomical images. Ophthalmic applications have also benefited from these devices, allowing the recording of in vivo high resolution retinal images through the compensation of ocular aberrations [26]. The interest of the liquid crystal technology in adaptive optics for the study of the eye [27,10] has experienced a significant increase in the last decade, driven by successive improvements in terms of simplicity-of-use, resolution, speed and cost. Along this line, a number of experiments have showed the potential of adaptive optics, initially intended for aberration correction, with the capability of manipulating the wavefront for a better understanding of vision. Neural effects associated with adaptation to the subjects' ocular aberrations have been reported in recent years using adaptive optics visual simulators [28,29,30,31]. Deformable mirrors have been mainly used in visual simulators, although liquid crystal phase modulators have also showed an important potential [32,33,34]. The large number of independent pixels for producing a given phase [35] allows programming not only continuous phase patterns, but almost any type of wavefront. Local discontinuities can be in principle generated with these devices. This feature of the liquid crystal modulators, technically impossible with continuous flexible mirrors, provides the necessary tool for exploring exotic phase profiles which could have an impact in the design of advanced ophthalmic optics elements [32]. The capability for reproducing discontinuous phase profiles has also permitted the use of these devices in optical trapping, where holographic and diffractive masks need to be generated [36,37].

One of the most remarkable advances in the use of liquid crystal for phase modulation reported in the last years has been the introduction of the on-Silicon technology [38-41]. Essentially, in the new devices the liquid crystal molecules alignment, and therefore the local refractive index, is controlled by a CMOS (Complementary Metal Oxide Semiconductor) sheet directly placed below the liquid crystal layer. A fundamental difference with the previous technology is the increase in the response velocity of the device. Twisted nematic liquid crystal could now be driven at rates up to 60 Hz. The liquid crystal on Silicon (LCOS) technology opens new possibilities and applications for the liquid crystal in different fields where faster responses are required. In the particular case of ophthalmic applications, the human eye exhibits temporal dynamic characteristics mostly between 5 and 10 Hz [42-43]. Previous liquid crystal devices hardly allowed temporal rates in this range, therefore real time correction or modification of the ocular aberrations was restricted. With the new LCOS phase modulators, true real time aberration correction becomes possible. The high fidelity inherent to the liquid crystal modulators also permits their operation in open loop, with no need of feedback for achieving the intended final wavefront. An important issue for any correcting device, particularly if it is intended to be used in open loop, is the characterization of the aberration generation. Several works have faced this task from different perspectives [2,27,8,10]. Aberrations are commonly expressed in terms of the Zernike polynomial expansion [44]. Consequently, knowing the ranges of accurate generation of those

polynomials is fundamental information when working with the LCOS phase modulator. Using the correcting device implemented in an adaptive optics system makes difficult to truly asses the actual limits of performance, since closed-loop systems are self-contained. In a previous work [10] we employed a Hartmann-Shack wavefront sensor [45,46,47] for finding the ranges of production of the Zernike polynomials in an optically-addressed liquid crystal phase modulator. The estimation of the generated wavefront was then validated by recording associated point spread functions with an additional optical relay, independent from the closed loop system. For aberration values beyond the production range an intensity peak at the paraxial focus was found in the point-spread images. The origin of this artifact lies on diffraction effects. The phase modulator begins to behave as a diffraction grating as the distance between two phase wrappings tends to the modulator pixel size. Actually, the paraxial peak represents the order zero of the diffracted wavefront. Hartmann-Shack wavefront estimations tend to minimize this effect and therefore to overestimate the accurate aberration production ranges, as measured in our previous study [10]. The existence of this paraxial peak when large, and perhaps moderate, aberrations are programmed in the phase modulator might have an impact in adaptive optics for high resolution imaging purposes. The aberration correction would be in that case less effective. Furthermore, the paraxial peak would have an even larger impact for adaptive optics visual simulators, since the subject would potentially see a paraxial replica of the object together with an aberrated image. In the current work, we propose an alternative method for characterizing the effective range of production of aberrations for a LCOS phase modulator device (LCOS-SLM X10468, Hamamatsu, Japan). It is based on the comparison between optically degraded and digitally obtained images for varying amounts of pure Zernike modes. This comparison is not performed directly between pairs of images, but through the calculation of the two dimensional correlation coefficient of each degraded image and the original one instead. From these calculations, we systematically obtained the range of values accurately generated by the LCOS phase modulator for each Zernike polynomial with no noticeable diffractive artifacts.

2. Methods

2.1 Experimental recording of aberrated images

The LCOS phase modulator device operates as an external monitor of a computer where the desired phase maps are displayed via a DVI (Digital Visual Interface) connector. Measurements of the temporal response of the device were conducted prior to its incorporation in the set-up. We obtain a very good agreement between our results and the technical specifications given by the manufacturer, being the typical time for rise and fall 10 and 30 ms, respectively. In order to generate the required images, the LCOS phase modulator has to be first calibrated. The calibration procedure is analogous to that for an optically-addressed PPM, described elsewhere [10]. The gray level-to-phase gain was evaluated by fitting a sinusoidal function to the transmitted intensity for a series of flat images displayed in the phase modulator operated in mode of intensity modulation, i.e., with the modulator between two polarizers with the transmission axis rotated 45º with respect to the liquid crystal orientation axis. Since the transmitted intensity was recorded with a camera imaging the modulator surface, the calibration was performed locally. The coefficient of variation, standard deviation divided by mean, was lower than 2%, meaning that the gray level-to-phase gain was virtually constant across the liquid crystal surface. Accordingly, a single global value was used for the gain. The averaged intensity fitting which produces that global value is presented in Fig. 1. The LCOS phase modulator model was a prototype designed to work in blue light, whose characteristics where relatively similar as those of the currently available model X10468-04. The functional wavelength range (capable of full 2π modulation) was slightly smaller in our prototype. Accordingly, we selected for the experiment a readout light wavelength of 488 nm.
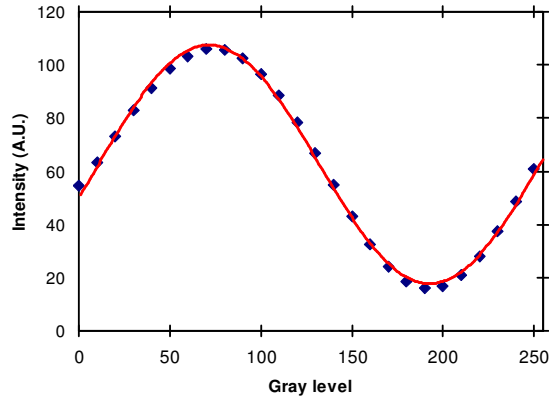
Fig. 1. Average intensity recorded for a series of flat images with different gray level displayed by the LCOS phase modulator, in pure intensity modulation mode. The gray level-to-phase gain is 0.0259 ± 0.0003 rad / gray level. A 2π phase is achieved with an 8-bit gray level of 242.5 ± 2.5. Readout light wavelength: $\lambda = 488$ nm.

The capability of the LCOS phase modulator for introducing different phase patterns was studied through the recording of images corrupted by different types and amounts of aberrations. The Zernike polynomials up to the fifth order were individually studied. The LCOS phase modulator was programmed for generating the phase profile of each Zernike polynomial with amplitudes ranging from - 4 to 4 µm, in 0.2 µm steps. For some selected cases, (vertical coma aberration, $Z(3,-1)$ and spherical aberration $Z(4,0)$ in double index OSA notation), a finer 0.1 µm step sampling was performed. The object was the USAF 1954 resolution test target.

The experimental system is shown in Fig. 2. A halogen bulb light was coupled into a multimode optical fiber for illuminating the resolution test. Oblique illumination with an angle of approximately 30 deg referred to the plane of the object prevented the weak specular component produced by the test from entering the system. The test irradiance was not homogeneous. However, assuming near perfect diffusion by the USAF test, the illumination structure should have no impact on the experiment. Wavelength was selected by an interference filter of 10 nm bandwidth centered at 488 nm. An achromatic doublet of 100 mm focal length, L1, served as objective producing an image of the resolution target at infinite. The LCOS phase modulator was placed at the focal length of the objective. A telescope composed of two doublets of focal lengths 100 and 80 mm (L2 and L3, respectively), conjugated the plane of the LCOS phase modulator with the exit pupil of the system. The latter was a diaphragm of 8.4 mm in diameter, corresponding to 10.5 mm on the LCOS phase modulator plane. A linear polarizer P was placed before the diaphragm to select the appropriate component of the light. A final achromatic doublet of 50 mm of focal length, L4, next to the diaphragm formed the image of the USAF test on a CCD camera located at its focal plane. 14 bit images were recorded by means of a DV887 front illuminated EMCCD camera (Andor Technology, USA) comprising a 512x512 pixels CCD sensor (pixel size of 16 µm). Exposure time was set to 0.5 s. This relatively high value was imposed by both the low irradiance from the light source at 488 nm and the modest spectral response of the sensor itself at the selected wavelength. The quantum efficiency of the CCD at 488 nm was approximately 10 % of its maximum.
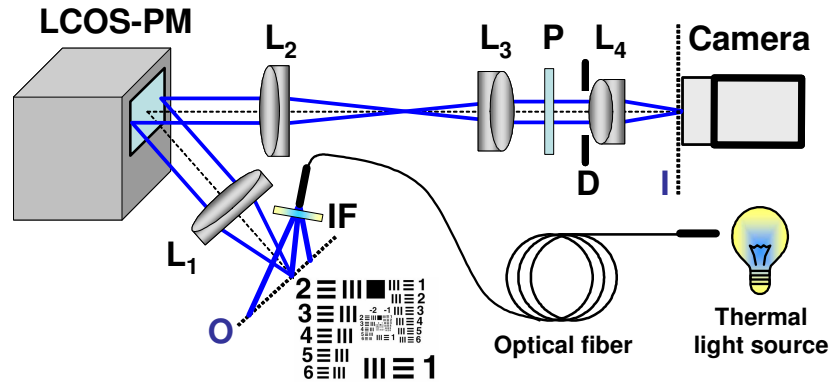
Fig. 2. Experimental set-up. The LCOS phase modulator was used to degrade the images of the USAF test recorded by the CCD camera. A telescope formed by lenses L2 and L3 conjugated the plane of the liquid crystal to the exit pupil of the imaging system. An interference filter (IF) centered at 488 nm was inserted in front of the optical fiber in order to illuminate the test with monochromatic light. A polarizer (P) with the transmission axis aligned with the liquid crystal molecule orientation was required for phase modulation.

2.2 Calculations of the aberrated images

In order to determine the LCOS phase modulator performance for aberration generation, the series of experimental images optically degraded for each Zernike polynomial up to fifth order were compared to their respective digitally generated counterparts. The characterization of the performance of the correcting device in terms of Zernike polynomials is mathematically arbitrary. They were selected since they are nowadays the standard way for describing aberrations in circular pupils. The resolution target was digitally blurred by convolution with the appropriate point spread function (PSF). Rigorously, the object for the convolution should be the USAF resolution test modulated by the illumination structure. In practice, we used the experimental image for zero aberrations (flat phase map displayed into the LCOS phase modulator) as object instead. Although this image corresponds to a filtered version of the object, in our case this was a minor issue due to the CCD camera resolution: the calculated Airy spot diameter for the system geometry and dimensions was 7.08 µm while the CCD pixel size was 16 µm. Consequently, the diffraction effects for zero aberrations were inferior to the sensibility of the detector and should have no practical effect in this study.

The PSFs corresponding to each Zernike polynomial were obtained through Fourier transform of their corresponding generalized pupil functions [48,49]. The aberration maps were generated and Fourier transformed with a high sampling ratio. The resulting PSF was re-sampled to the equivalent pixel size actually occurring on the CCD. The procedure rendered an effective loss of information, emulating the actual recording of the degraded images. The method is illustrated in Fig. 3. Top left panel shows the 2π-wrapped representation of 1 µm of horizontal coma aberration, $Z(3,1)$, selected as an example. This aberration map can be displayed into the LCOS phase modulator in order to record the optically degraded image. The central 250×250 pixel zone of this image can be seen in the bottom left panel, color-coded maximizing contrast from blue (low intensity) to red (high intensity). Top right panel in Fig. 3, displays the theoretical PSF calculated from the aberration map, digitally zoomed by a factor of 2.5 for better visualization. The re-sampling of the PSF to match the CCD pixel size results in a noticeable pixilation. The resulting PSF was then convolved with the image zero aberrations in order to obtain the digitally aberrated image (bottom tight panel). The procedure was systematically repeated for every Zernike polynomial and for the same set values used for recording experimental images.

Wave aberration (LCOS)

PSF (digital)

x 2.5

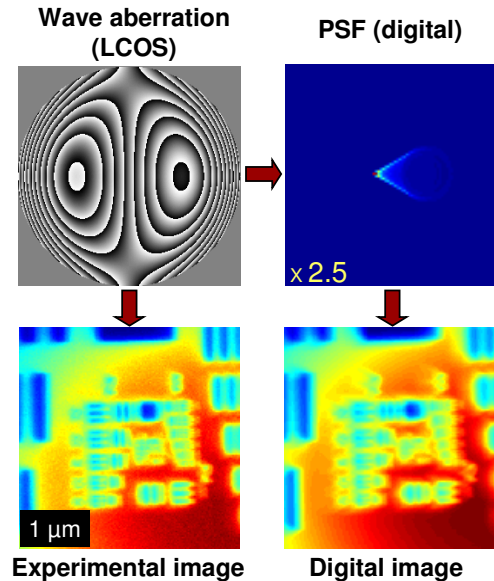**Experimental image**

1 μm

Digital image

Fig. 3. Schematics of the procedure for obtaining experimental and digital images. The latter are generated by convolution of the calculated point spread function with the object. Experimental images are obtained with the optical system, degrading the wavefront with the LCOS phase modulator through the induction of aberrations.

2.3 Comparison of experimental and calculated sets of images

The aberration production range for the LCOS phase modulator is mainly limited by the apparition of diffractive artifacts. In particular, a 0-order diffraction peak has been observed to appear in the experimental PSFs as the aberration level increases [10]. The expected effect of this artifact on the degraded image of an object would be the apparition of a ghost version of the object on top of the correctly degraded image. The aim of our study is to check the aberration values for which diffraction peak becomes noticeable and has an impact on the image quality of the outcome. One approach to pursue this aim could be the comparison of each experimentally degrade image with its corresponding computed counterpart. Different approaches for comparing two set of images are available in the literature [50-53]. The purpose of confronting the two sets in our work was not finding subtle differences between images, but to establish ranges for accurate use of the LCOS phase modulator. By comparing the two bottom panels in Fig. 3, the presence of noise in the experimental image is evident. That could make difficult the comparison between pairs of images.

The alternative approach we selected was the confrontation of the degradation tendency of the series of images with respect to the non-degraded series. This course of action requires a function of merit to quantify the progressive degradation of the final image when aberrations increase. We selected the correlation coefficient with the zero-aberration image. This statistical parameter presents advantages in terms of simplicity and computing time for the required task. Accordingly, we systematically obtained the two dimensional correlation coefficient between the original image and every degraded image from each set, i. e., the experimental and the digitally generated images. The correlation coefficient in the context of statistics provides an indicator of the strength or goodness of a linear relationship between two random variables. Correlation is usually normalized and ranges from zero to one, indicating the level of relationship between the variables. Zero value corresponds to the absence of relationship whilst one shows perfect linear match. In our case, the variables were the intensity patterns of the original and degraded images. The mathematical function describing the two dimensional correlation was given by:

$$C_2(A,B) \quad = \quad \frac{\langle A \cdot B \rangle - \langle A \rangle \cdot \langle B \rangle}{\left(\langle A^2 \rangle - \langle A \rangle^2 \right)^{1/2} \cdot \left(\langle B^2 \rangle - \langle B \rangle^2 \right)^{1/2}}$$

where A and B are the normalized intensities of the original and degraded images, and $\langle \, \rangle$ represents the average across pixels.

3. Results and discussion

The two dimensional correlation coefficient between each aberrated image degraded and the reference image of the object was systematically obtained. The procedure was repeated for both the experimental images and the theoretical or computationally obtained set of images. Direct comparison of the evolution of the correlation coefficient between the two sets of images was performed for each Zernike polynomial.

The results are summarized on Fig. 4, where selected polynomials are studied. In particular, results for a representative polynomial for each radial and azimuthal order are presented. The scale across all subplots in Fig. 4 is preserved. The red lines show the evolution of the correlation coefficient obtained from the digital images, while the blue curves correspond to the experimental images.
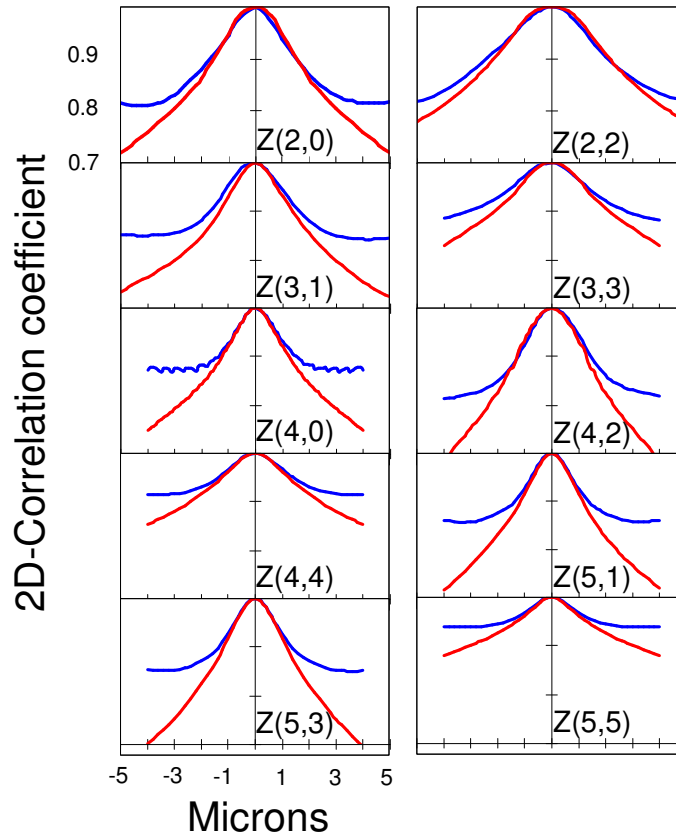

Fig. 4. Evolution of the two-dimensional correlation coefficient as a function of the amplitude of several Zernike coefficients. Red color indicates the function obtained from the set of digital images whilst blue corresponds to the experimental ones.

For every polynomial, there is a range of values where the evolution of the correlation obtained from both cases follows a similar trend. Systematically, the two curves matched for small and moderated values of the Zernike coefficients. These results suggest that up to a certain value of each Zernike coefficient, the optical degradation produced by LCOS phase modulator is close to the theoretical predictions. However, as the coefficient increases another region can be identified in every plot, where the difference between the theoretical and experimental curves becomes substantial. The correlation in the experimental set presents a progressive decreasing in the slope for both the positive and negative direction. In most of the cases, it is possible to notice a saturation or region where the experimental curve is essentially flat. On the contrary, the correlation for the digital image set consistently declines, as it can be expected for increasing levels of degradation, and exhibits only a slight change in slope within the considered range. This behavior produces a consequent increase in the difference towards the periphery between the experimental and the theoretical correlation curves.

The existence of a saturation level in the experimental curve can be attributed to the apparition of a ghost image due to the 0-order diffraction artifacts and, therefore, sets an effective threshold for the performance of the LCOS phase modulator, beyond which optical aberrations cannot be properly generated. The actual impact of the saturation over the images is illustrated in Fig. 5, which compares experimental and digitally aberrated images for some values of pure defocus aberration, $Z(2,0)$. The images degraded with low levels of defocus have a similar appearance. However, when comparing those associated to larger values of defocus, a mismatch between the digital and the experimental images can be seen. Actually, the experimental images show an apparent increase in resolution for the largest amounts of defocus introduced. As an example, the entire left column of numbers from 2 to 5 can be resolved in the image degraded by 4.4 µm of defocus. Compared to the image associated to the value 2.0 µm the increase in the quality of the former image is evident. This kind of behavior was systematically found for every Zernike polynomial. On the contrary, the theoretical set of images presents a monotonic increase in the degradation, with the consequent loss of resolution as a function of the Zernike coefficient. This different behavior is the cause of the progressive separation of the curves in Fig. 4.
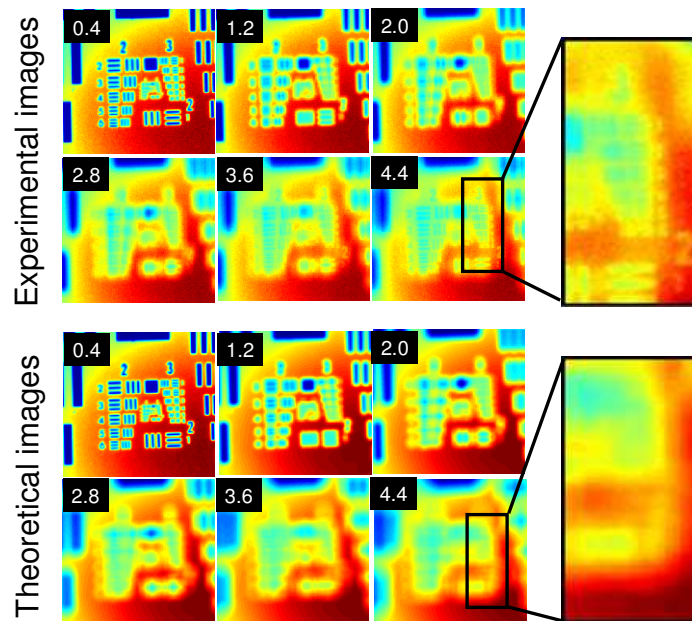

Fig. 5. Effect of introducing different values of pure defocus, Zernike Z(2,0), over the image in the experimental and the digital case.

The evolution of the correlation curves can therefore be related to the qualitative progression of image degradation. For small values of aberration, the induction of Zernike polynomials is correctly accomplished and the experimental and digital correlations virtually coincide. For larger aberration values the diffraction artifacts become noticeable from the point of view of effective image degradation and the difference between correlations increase. However, it is important to note that the decline in the aberration generation performance of the LCOS phase modulator is a gradual process and, consequently, so it is the separation between the theoretical and experimental correlation curves with no clear breakout point. Therefore, the determination of the aberration range for correct aberration induction has a subjective component. We selected a threshold value of 1.5% for the difference between the experimental and digital correlations. This value was selected after visual inspection of the image series for all the Zernike coefficients studied. In every case, the experimental images for Zernike coefficient values below this threshold closely resembled the digital ones, with no apparent diffraction ghost image. In order to smooth the noise and to avoid incongruous asymmetries, we chose to fit the difference between experimental and theoretical correlation to a 4th order even polynomial containing the origin. For every studied Zernike polynomial, r^2 was equal or better than 0.98. Figure 6 shows as a function of the Zernike polynomial the aberration values corresponding to the 1.5% threshold in the fitted correlation difference. Additionally, error bars are shown in Fig. 6, corresponding to the coefficient values that produced a 1% (lower limit) and a 2% (upper limit) difference between correlations.
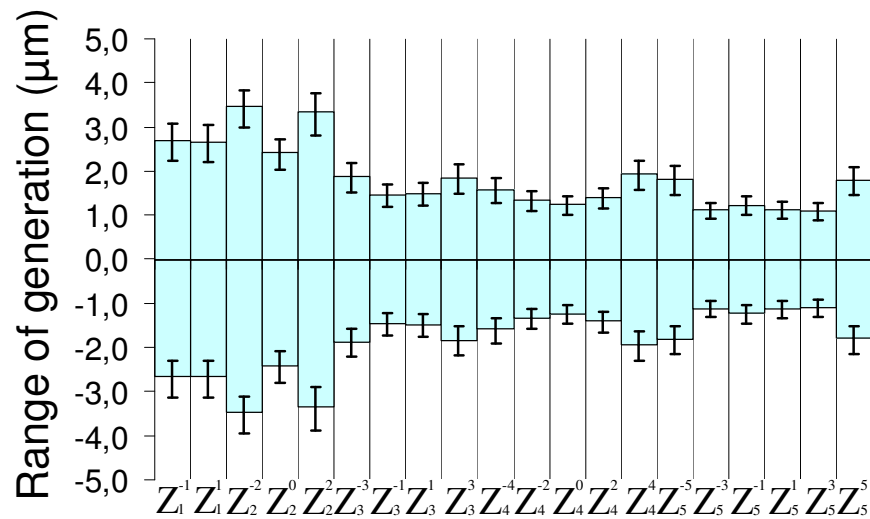

Fig. 6. Ranges of accurate aberration generation as a function of the Zernike polynomial, calculated as the coefficient values that produce a 1.5% difference between the experimental and digital correlation. Each value can be understood as the maximum amount of a given polynomial that can be induced by the LCOS phase modulator with no artifacts over the resulting degraded image. Error bars correspond to the coefficient values that produce a correlation difference between 1% and 2%.

The ranges of aberration production shown in Fig. 6 are basically symmetrical around 0. The LCOS phase modulator proves to be capable of accurately generating more than $\pm$ 1 μm of aberration for every tested Zernike mode, and the range exceeds $\pm$ 2 μm in several cases. It has to be pointed out that the aberrations are generated over a 10.5 mm pupil diameter in the LCOS phase modulator plane which is optically de-magnified into the exit pupil, increasing the relevance of these ranges. As an example, the $\pm$ 2.4 μm of defocus correspond to $\pm$ 0.94 D in our case due to the modest 0.8 magnification used (8.4 mm exit pupil) but would result in $\pm$ 4.16 D range for a 4 mm exit pupil (0.38 magnification).

When comparing the ranges of accurate aberration generation for different Zernike modes, a complex dependence on the Zernike indexes can be seen. There is a clear drop in performance from second to third order but the dependence with the radial order is not obvious for higher values of n. Inside each radial order, the range tend to increase with the azimuthal number regardless of its sign, so that the production ranges for $Z(n,m)$ and $Z(n,-m)$ are basically equivalent. The reason for this complex behavior probably lies in the different distribution of local phase slopes in each Zernike polynomial, which means that the diffraction artifacts become relevant for different coefficient values. Related with this idea, it is important to restate that the ranges in Fig. 6 correspond to the production of individual Zernike modes. When a combination of modes is considered, the occurrence of the diffraction artifacts will depend on the whole wavefront shape and, therefore, the individual range values cannot be expected to hold. The interaction between different modes is a complicated process [54] that will most probably lead to asymmetries and in some cases could even increase the production range for specific combinations of Zernike modes. The previous discussion refers to the experimental results obtained at wavelength 488 nm. It should be noted that since the appearance of the paraxial ghosts arises as a consequence of diffraction effects associated with phase wrapping, considering a different wavelength the ranges of production of Zernike polynomials would then change accordingly. Approximately the generation of aberrations ranges can be scaled by the ratio between the new wavelength and the reference wavelength 488 nm.

A potential limitation of the technique presented here for studying the degradation of the images is the existence of other static aberrations introduced by the system. Their effects would combine with those generated by the LCOS phase modulator. Fine alignment of the set-up largely avoids monochromatic aberrations. However, the two dimensional correlation exhibited a slightly asymmetric behavior for some polynomials (e.g., $Z(2,2)$ and $Z(3,1)$ in Fig. 4), which can probably be attributed to the presence of small amounts of aberrations degrading the original image. In any case, these asymmetries are slight and our fitting to an even function further reduces their potential impact on the calculated ranges. Field aberrations are rather more difficult to completely eliminate unless dedicated objectives are used, with the corresponding increase in complexity and cost of the experimental set-up. An alternative allowing the use of regular optics is the reduction of the imaged field. In our case we limited our analysis to the central 250×250 pixel area in the CCD, where no evident field curvature was observed.

A clear difference between the experimental and digital images is the noise present in the former ones. The incorporation of noise could render a more similar appearance of the digital images with respect to the experimental set. We tested the incorporation of zero-mean Gaussian white noise with different local variance values, finding a value of 0.00015 for the variance as the most convenient in terms of similarity between the digital images and the experimental ones. However, the merit function applied in this work for classifying the quality of the set of images was invariant to the addition of noise. Therefore, quantitative analysis was not enhanced with the addition of noise. Results obtained in figures 4 and 6 were identical with and without noise. This can be understood in terms of a practical balance of the added noise occurring in the entire image. Therefore, even though the digital set of images are qualitatively perceived as more similar to their corresponding experimental counterparts, the addition of noise did not change the ranges shown in Fig. 6.

4. Conclusions

In this work we investigate the capabilities of a LCOS phase modulator for aberration manipulation. We developed an imaging system for recording extended images of an USAF test in order to study the degradation experimentally produced when the LCOS phase modulator is used as an aberration generator. Degraded images were recorded for pure Zernike modes covering the whole set up to 5th order, in each case with values ranging from -4 to 4 µm in 0.2 µm steps. Additionally and for comparison purposes, series of digitally

degraded images were produced by convolution of the initial non-degraded image with the theoretical PSFs computed for each aberration value. Both for the experimental and digital sets, image degradation was quantified by means of the two dimensional correlation coefficient with respect to the original image with no aberrations induced. In order to check the device reliability, the behavior of the correlation coefficient for the experimental set of images was compared with its digital counterpart. In every case, there is a good match for low aberration values that tends to deteriorate beyond a certain value, allowing us to define the range of accurate aberration manipulation for each Zernike mode.

The LCOS phase modulator is a promising technology for adaptive optics applications, comprising the typical advantages of liquid crystal modulators, e.g., high resolution, high fidelity and potential low cost, while solving the major drawback of previous liquid crystal devices: the slow response time. It must be said that the capability of refreshing rates of up to 60 Hz notably enhances the performance of previous liquid crystal devices, although it is still far from the kHz range currently available in other types of aberration correctors, as electrostatic or bimorph deformable mirrors for instance. The use of linearly polarized light is irrelevant in the context of vision and ocular aberrations [55]. Nevertheless, polarization and their moderate temporal response make such correctors inefficient for astronomical applications. The ranges for accurate production of Zernike polynomials obtained in the present work should be observed when using the LCOS phase modulator as aberration corrector or generator in adaptive optics. In particular, for experiments of visual simulation, involving a visual task combined with simultaneous manipulation of the wavefront, compliance with the obtained aberration limits should avoid the apparition of the paraxial replica that could disturb the visual outcomes.

Acknowledgments